SLAC-PUB-14832

Gymnastics in Phase Space

Alexander Wu Chao[1]
SLAC National Accelerator Laboratory
2575 Sand Hill Road, Menlo Park, CA 94025, USA

Abstract

As accelerator technology advances, the requirements on accelerator beam quality become increasingly demanding. Facing these new demands, the topic of phase space gymnastics is becoming a new focus of accelerator physics R&D. In a phase space gymnastics, the beam's phase space distribution is manipulated and precision tailored to meet the required beam qualities. On the other hand, all realization of such gymnastics will have to obey accelerator physics principles as well as technological limitations. Recent examples of phase space gymnastics include Emittance exchanges, Phase space exchanges, Emittance partitioning, Seeded FELs and Microbunched beams. The emittance related topics of this list are reviewed in this report. The accelerator physics basis, the optics design principles that provide these phase space manipulations, and the possible applications of these gymnastics, are discussed. This fascinating new field promises to be a powerful tool of the future.

1 Introduction

As we demand more and more from accelerators, beam manipulation techniques get more advanced, and phase space gymnastics has evolved to become a critical topic in accelerator physics. Just like the physical gymnastics, e.g. in the Olympic games, the skills needed in phase space gymnastics are highly technical and precise, while the resulting performance exquisite and beautiful. The ability to manipulate the beam's 6D phase space offers many precision oriented operations of the beam, and opens up many applications, e.g. for linear colliders and FELs. This is a new and very fertile R&D field.

Earlier phase space gymnastics have been mostly applied to the 2D longitudinal phase space, and took the form of RF manipulations in beam injection, extraction, and phase space displacement acceleration [1]. The recent advances, led by the seminal papers by Derbenev [2], begin to incorporate the transverse dimensions and become much more sophisticated, yielding a new wealth of additional applications. This new development has so far led to the inventions of Adapters, Emittance exchanges, Phase space exchanges, and various Emittance partitioning techniques. We will discuss these emittance related topics in this

[1]Work supported by DoE contract D-AC02-76SF00515

report. The other new phase space manipulations applied to various seeded and microbunching techniques for the free electron lasers are not contained in this report.

The idea of flat-to-round and round-to-flat adapters was first introduced by Derbenev [2] and later rapidly extended by him and many others [3]-[13]. Derbenev first envisioned applying it to a storage ring collider to form round beams at the collision point to mitigate the effect of the encountered beam-beam nonlinear resonances. This idea has also been considered for electron cooling [3, 7]. The production of a very flat beam from a round photocathode immersed in a solenoid followed by a round-to-flat adapter has been experimentally demonstrated [10, 11, 12]. During this time, several other kinds of adapters have been invented, including emittance exchange adapters and phase space exchange adapters [14]-[22]. Non-symplectic applications for emittance partitioning have also been developed [23]-[25].

Phase space gymnastics permit precision manipulations because phase space is conserved. Liouville theorem is the root cause of this phase space technology.

2 Adapters

Consider the 4D canonical phase space $X_{\rm can} = (x, p_x, y, p_y)$. We have two representations to describe particle motion in this phase space:

1. For uncoupled case, use the Courant-Snyder basis of planar modes (x and y modes) in a familiar matrix form [26]:

$$X_{\rm can} = Va \tag{1}$$

where

$$V = \begin{bmatrix} \sqrt{\beta_x}\cos\phi_x & \sqrt{\beta_x}\sin\phi_x & 0 & 0 \\ \frac{-\alpha_x\cos\phi_x - \sin\phi_x}{\sqrt{\beta_x}} & \frac{-\alpha_x\sin\phi_x + \cos\phi_x}{\sqrt{\beta_x}} & 0 & 0 \\ 0 & 0 & \sqrt{\beta_y}\cos\phi_y & \sqrt{\beta_y}\sin\phi_y \\ 0 & 0 & \frac{-\alpha_y\cos\phi_y - \sin\phi_y}{\sqrt{\beta_y}} & \frac{-\alpha_y\sin\phi_y + \cos\phi_y}{\sqrt{\beta_y}} \end{bmatrix} \tag{2}$$

and

$$a = \begin{bmatrix} \sqrt{2\epsilon_x}\sin\chi_x \\ \sqrt{2\epsilon_x}\cos\chi_x \\ \sqrt{2\epsilon_y}\sin\chi_y \\ \sqrt{2\epsilon_y}\cos\chi_y \end{bmatrix} \tag{3}$$

These equations describe the motion of particles in a planar beamline whose x- and y beam emittances are ϵ_x, ϵ_y. Lattice functions $\alpha_{x,y}, \beta_{x,y}, \phi_{x,y}$ are the familiar betatron parameters in this representation; $\chi_{x,y}$ are the initial betatron phase of the particle under consideration.

2. For a fully coupled beam with rotational symmetry (e.g. in a solenoidal field), one can describe particle motion using the basis of circular modes (left-handed and right handed modes) [8]:

$$X_{\rm can} = Ub \tag{4}$$

where

$$U = \frac{1}{\sqrt{2}} \begin{bmatrix} \sqrt{\beta}\cos\phi_+ & \sqrt{\beta}\sin\phi_+ & -\sqrt{\beta}\cos\phi_- & -\sqrt{\beta}\sin\phi_- \\ \frac{-\sin\phi_+ - \alpha\cos\phi_+}{\sqrt{\beta}} & \frac{\cos\phi_+ - \alpha\sin\phi_+}{\sqrt{\beta}} & \frac{\sin\phi_- + \alpha\cos\phi_-}{\sqrt{\beta}} & \frac{-\cos\phi_- + \alpha\sin\phi_-}{\sqrt{\beta}} \\ \sqrt{\beta}\sin\phi_+ & -\sqrt{\beta}\cos\phi_+ & \sqrt{\beta}\sin\phi_- & -\sqrt{\beta}\cos\phi_- \\ \frac{\cos\phi_+ - \alpha\sin\phi_+}{\sqrt{\beta}} & \frac{\sin\phi_+ + \alpha\cos\phi_+}{\sqrt{\beta}} & \frac{\cos\phi_- - \alpha\sin\phi_-}{\sqrt{\beta}} & \frac{\sin\phi_- + \alpha\cos\phi_-}{\sqrt{\beta}} \end{bmatrix} \tag{5}$$

and

$$b = \begin{bmatrix} \sqrt{2\epsilon_+}\sin\chi_+ \\ \sqrt{2\epsilon_+}\cos\chi_+ \\ \sqrt{2\epsilon_-}\sin\chi_- \\ \sqrt{2\epsilon_-}\cos\chi_- \end{bmatrix} \tag{6}$$

for a beam with left-handed and right-handed emittances ϵ_+ and ϵ_-. Lattice parameters are $\alpha, \beta, \phi_+, \phi_-$, i.e., there is only one β-function but two (left-handed and right-handed) phases.

Once we have the planar basis V and the circular basis U — both are symplectic — we can now consider "adapters".

2.1 Flat-to-flat adapters

Flat-to-flat adapter from s_1 to s_2 is well known. The job is to design a lattice that provides the map from $V(s_1)$ to $V(s_2)$, i.e. the optics matching from one set of lattice parameters to another. A moment's reflection shows that the needed matching map is given by $V(s_2)V(s_1)^{-1}$, and a simple calculation gives

$$V(s_2)V(s_1)^{-1} = \begin{bmatrix} \sqrt{\frac{\beta_{x2}}{\beta_{x1}}}(\cos\mu_x + \alpha_{x1}\sin\mu_x) & \sqrt{\beta_{x1}\beta_{x2}}\sin\mu_x & 0 & 0 \\ \frac{(\alpha_{x1}-\alpha_{x2})\cos\mu_x - (1+\alpha_{x1}\alpha_{x2})\sin\mu_x}{\sqrt{\beta_{x1}\beta_{x2}}} & \sqrt{\frac{\beta_{x1}}{\beta_{x2}}}(\cos\mu_x - \alpha_{x2}\sin\mu_x) & 0 & 0 \\ 0 & 0 & \sqrt{\frac{\beta_{y2}}{\beta_{y1}}}(\cos\mu_y + \alpha_{y1}\sin\mu_y) & \sqrt{\beta_{y1}\beta_{y2}}\sin\mu_y \\ 0 & 0 & \frac{(\alpha_{y1}-\alpha_{y2})\cos\mu_y - (1+\alpha_{y1}\alpha_{y2})\sin\mu_y}{\sqrt{\beta_{y1}\beta_{y2}}} & \sqrt{\frac{\beta_{y1}}{\beta_{y2}}}(\cos\mu_y - \alpha_{y2}\sin\mu_y) \end{bmatrix} \tag{7}$$

Equation (7) of course is a well known result; $\mu_x = \phi_{x2} - \phi_{x1}, \mu_y = \phi_{y2} - \phi_{y1}$ are the betatron phase advances from s_1 to s_2. A particle with initial condition (3) is now brought from position s_1 to position s_2.

2.2 Round-to-round adapters

Round-to-round adapter from s_1 to s_2, i.e., from one set of circular lattice parameters to another is given by the map $U(s_2)U(s_1)^{-1}$. Although the algebra is somewhat involved, it can be shown that the result can be written as

$$U(s_2)U(s_1)^{-1} = R(\theta)T \tag{8}$$

where $R(\theta)$ is a rotation matrix with rotation angle θ,

$$R(\theta) = \begin{bmatrix} \cos\theta & 0 & \sin\theta & 0 \\ 0 & \cos\theta & 0 & \sin\theta \\ -\sin\theta & 0 & \cos\theta & 0 \\ 0 & -\sin\theta & 0 & \cos\theta \end{bmatrix} \tag{9}$$

and

$$T = \begin{bmatrix} \sqrt{\frac{\beta_2}{\beta_1}}(\cos\mu + \alpha_1 \sin\mu) & \sqrt{\beta_1\beta_2}\sin\mu & 0 & 0 \\ \frac{(\alpha_1-\alpha_2)\cos\mu-(1+\alpha_1\alpha_2)\sin\mu}{\sqrt{\beta_1\beta_2}} & \sqrt{\frac{\beta_1}{\beta_2}}(\cos\mu - \alpha_2\sin\mu) & 0 & 0 \\ 0 & 0 & \sqrt{\frac{\beta_2}{\beta_1}}(\cos\mu + \alpha_1\sin\mu) & \sqrt{\beta_1\beta_2}\sin\mu \\ 0 & 0 & \frac{(\alpha_1-\alpha_2)\cos\mu-(1+\alpha_1\alpha_2)\sin\mu}{\sqrt{\beta_1\beta_2}} & \sqrt{\frac{\beta_1}{\beta_2}}(\cos\mu - \alpha_2\sin\mu) \end{bmatrix} \tag{10}$$

The left-handed and right-handed betatron phases at s_2 are then given by $\phi_{+2} = \phi_{+1} + \mu - \theta$ and $\phi_{-2} = \phi_{-1} + \mu + \theta$.

There are two ways to accomplish this desired map (8):

- a quadrupole channel that provides the map (10), followed by rotating the entire subsequent beamline (not including the quadrupole channel) by $-\theta$.
- A uniform solenoid with strength k_s and length z (including its two ends) will produce this map with $\theta = \mu = k_s z/2, \beta_1 = \beta_2 = 2/k_s, \alpha_1 = \alpha_2 = 0$.

2.3 Round-to-flat adapters

A round-to-flat adapter is given by the map $U(s_2)V(s_1)^{-1}$, which can be shown to have a general form of a round-to-round adapter, followed by a round-to-flat insertion with map $(UV^{-1})_0$, followed by a flat-to-flat adapter,[2] where $(UV^{-1})_0$

[2]For completeness, the needed round-to-round transformation is from $(\alpha, \beta, \phi_+, \phi_-)$ to $(\alpha = 0, \beta, \phi_+ = \phi_y + \mu - \pi/4, \phi_- = \phi_y + \mu + \pi/4)$. The needed round-to-flat transformation $(VU^{-1})_0$ is from $(\alpha = 0, \beta, \phi_+ = \phi_y + \mu - \pi/4, \phi_- = \phi_y + \mu + \pi/4)$ to $(\alpha_x = \alpha_y = 0, \beta_x = \beta_y, \phi_x = \phi_y)$. The needed flat-to-flat transformation from $(\alpha_x = \alpha_y = 0, \beta_x = \beta_y, \phi_x = \phi_y)$ to $(\alpha_x, \beta_x, \phi_x, \alpha_y, \beta_y, \phi_y)$. Combining all steps, we then have finally an adapter from $(\alpha, \beta, \phi_+, \phi_-)$ to $(\alpha_x, \beta_x, \phi_x, \alpha_y, \beta_y, \phi_y)$. Each step, although stated in language of mathematics, is directly translatable to conventional lattice designs.

has a simple form [3, 9, 10]

$$(UV^{-1})_0 = R\left(\frac{\pi}{4}\right)\begin{bmatrix} \sqrt{\frac{\beta}{\beta_y}}\cos\mu & \sqrt{\beta\beta_y}\sin\mu & 0 & 0 \\ -\frac{\sin\mu}{\sqrt{\beta\beta_y}} & \sqrt{\frac{\beta_y}{\beta}}\cos\mu & 0 & 0 \\ 0 & 0 & \sqrt{\frac{\beta}{\beta_y}}\sin\mu & -\sqrt{\beta\beta_y}\cos\mu \\ 0 & 0 & \frac{\cos\mu}{\sqrt{\beta\beta_y}} & \sqrt{\frac{\beta_y}{\beta}}\sin\mu \end{bmatrix} R\left(-\frac{\pi}{4}\right) \tag{11}$$

It is easy to see that $(UV^{-1})_0$ represents a regular quadrupole channel (miminum of three quadrupoles in general) rotated 45°. The 45° rotation renders the quadrupoles skew quadrupoles. Design of the adapter therefore reduces to a regular lattice matching problem.

Inserting a round-to-flat adapter brings a beam from a round optics with $(\alpha, \beta, \phi_+, \phi_-)$ to a flat optics with $(\alpha_x, \beta_x, \phi_x, \alpha_y, \beta_y, \phi_y)$. A round beam with left-handed and right-handed emittances of (ϵ_+, ϵ_-) is transformed to a planar beam with x- and y-emittances given by $(\epsilon_x = \epsilon_+, \epsilon_y = \epsilon_-)$.

2.4 Flat-to-round adapter

Reversing the round-to-flat adapter, a flat beam with x- and y-emittances of (ϵ_x, ϵ_y) is transformed to a round beam with left-handed and right-handed-emittances $(\epsilon_+ = \epsilon_x, \epsilon_- = \epsilon_y)$. This adapter can also be achieved by three skew quadrupoles.

2.5 Applications of flat-to-round and round-to-flat adapters

As mentioned, the idea of adapters was first introduced by Derbenev 1993 to control the beam-beam effect in storage ring colliders. But it has subsequently been much extended for other applications.

Storage ring colliders In this collider application [2], a planar flat beam in regular arc cells is transformed by a flat-to-round adapter to become a round beam at the collision region. The collision region is immersed in a solenoidal field. After the collision region, the beam is brought back to the regular arc by a round-to-flat adapter. With a round beam at the collision point, this possibly reduces the beam-beam effect due to much reduced number of nonlinear resonances.

Linear colliders In this application [5], a round beam is produced at the cathode immersed in a solenoidal field. After exiting the solenoid, a round-to-flat adapter transforms the beam into a flat planar configuration, which is what is needed for linear collider applications. The use of adapter here avoids the need of a damping ring to provide flat beams.

Relativistic electron beam cooling Applying a flat-to-round adapter to a very flat beam ($\epsilon_x \gg \epsilon_y$), a round beam can be produced with $\epsilon_+ \gg \epsilon_-$. Immersing the beam in a matched solenoid with appropriate magnetic field, particles in the beam will move in the solenoid with very small angular divergence, i.e., the beam becomes extremely laminar with all particles moving almost straight ahead along the solenoidal field with zero Larmor radius and as a result almost zero temperature. This is an ideal beam for performing electron cooling [3, 7].

Diffraction limited synchrotron radiation facility The electron cooling configuration can be installed in a synchrotron radiation storage ring. By an insertion with the configuration (flat-to-round adapter + solenoid + round-to-flat adapter), a conventional 3rd generation synchrotron radiation storage ring can reach diffraction limit for X-rays [6, 13] without a push to achieve the ultra-small emittances aimed by the "ultimate rings" [27].

For any given ring lattice that is able to produce a flat beam with $\epsilon_y \ll \epsilon_x$, one can in principle produce a round beam inside a solenoid with extremely small angular divergence. The full insertion consists of the solenoid and three adapter skew quadrupoles on each side. A coherent X-ray radiator is then inserted inside the solenoid.

3 Emittance and Phase space exchangers

There are more adapter types than mentioned so far. For example, one may stay with flat-to-flat, but wish to exchange the x and y coordinates. This means we want an adapter that transforms the base vectors from V of Eq.(2) at position s_1 to

$$V' = \begin{bmatrix} 0 & 0 & \sqrt{\beta_{x2}}\cos\phi_{x2} & \sqrt{\beta_{x2}}\sin\phi_{x2} \\ 0 & 0 & \frac{-\alpha_{x2}\cos\phi_{x2}-\sin\phi_{x2}}{\sqrt{\beta_{x2}}} & \frac{-\alpha_{x2}\sin\phi_{x2}+\cos\phi_{x2}}{\sqrt{\beta_{x2}}} \\ \sqrt{\beta_{y2}}\cos\phi_{y2} & \sqrt{\beta_{y2}}\sin\phi_{y2} & 0 & 0 \\ \frac{-\alpha_{y2}\cos\phi_{y2}-\sin\phi_{y2}}{\sqrt{\beta_{y2}}} & \frac{-\alpha_{y2}\sin\phi_{y2}+\cos\phi_{y2}}{\sqrt{\beta_{y2}}} & 0 & 0 \end{bmatrix} \tag{12}$$

at position s_2. The adapter needs to provide the map $V'(s_2)V^{-1}(s_1)$ — we omit the explicit calculation here. Obviously, when $\alpha_{x2} = \alpha_{y1}, \alpha_{y2} = \alpha_{x1}, \beta_{x2} = \beta_{y1}, \beta_{y2} = \beta_{x1}, \phi_{x2} = \phi_{y1}$ and $\phi_{y2} = \phi_{x1}$, we will have

$$V'V^{-1} = \begin{bmatrix} 0 & 0 & 1 & 0 \\ 0 & 0 & 0 & 1 \\ 1 & 0 & 0 & 0 \\ 0 & 1 & 0 & 0 \end{bmatrix} \tag{13}$$

One way to produce the map (13) is a solenoid with $k_s z = \pi$, followed by a normal quadrupole channel of

$$\begin{bmatrix} 0 & -\frac{2}{k_s} & 0 & 0 \\ \frac{k_s}{2} & 0 & 0 & 0 \\ 0 & 0 & 0 & \frac{2}{k_s} \\ 0 & 0 & -\frac{k_s}{2} & 0 \end{bmatrix} \tag{14}$$

When inserted, this adapter will cause x- and y-emittances to be exchanged.

One can also exchange x and z instead of x and y. Consider a planar lattice in $X = (x, x', z, \delta)$ coordinates. Let the transformation map be

$$\begin{bmatrix} A & B \\ C & D \end{bmatrix}$$

where A, B, C and D are 2×2 matrices. An *emittance exchanger* (EEX) requires $A = D = 0$ and it provides an exchange between the two phase spaces (x, x') and (z, δ). A *phase space exchanger*, on the other hand, requires not only $A = D = 0$ but also B and C = diagonal. It provides a cleaner exchange between x and z, and between x' and δ (variations are also possible).

3.1 Cornacchia-Emma EEX

The first EEX proposed by Cornacchia and Emma [14] is shown as the chicane scenario in Fig. 1 [19]. It consists of a simple 4-dipole chicane and a transverse cavity.

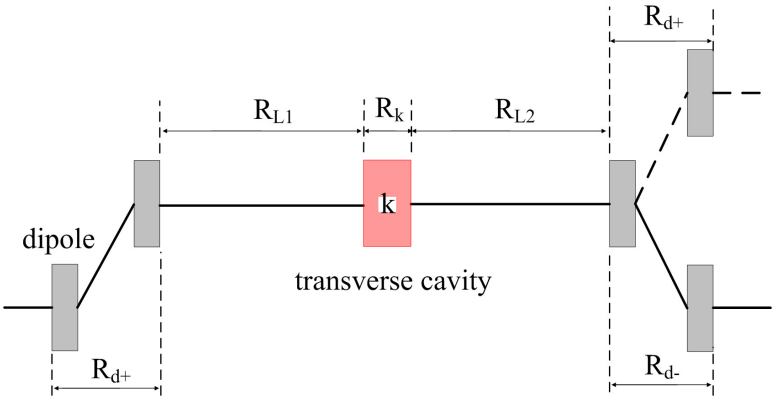

Figure 1: Emittance exchange beam line based on a chicane (the Cornacchia-Emma EEX) and two dog-legs (the Kim EEX).

The transfer matrix for the beamline is (the first and the fifth matrices are the two dog-legs on the two sides; η and ξ are the dispersion and the momentum compaction contributions from a dog-leg; the middle matrix represents the

transverse cavity with strength k)

$$\begin{bmatrix} 1 & L & 0 & -\eta \\ 0 & 1 & 0 & 0 \\ 0 & -\eta & 0 & \xi \\ 0 & 0 & 0 & 1 \end{bmatrix} \begin{bmatrix} 1 & L_2 & 0 & 0 \\ 0 & 1 & 0 & 0 \\ 0 & 0 & 1 & 0 \\ 0 & 0 & 0 & 1 \end{bmatrix} \begin{bmatrix} 1 & 0 & 0 & 0 \\ 0 & 1 & k & 0 \\ 0 & 0 & 1 & 0 \\ k & 0 & 0 & 1 \end{bmatrix} \begin{bmatrix} 1 & L_1 & 0 & 0 \\ 0 & 1 & 0 & 0 \\ 0 & 0 & 1 & 0 \\ 0 & 0 & 0 & 1 \end{bmatrix} \begin{bmatrix} 1 & L & 0 & \eta \\ 0 & 1 & 0 & 0 \\ 0 & \eta & 0 & \xi \\ 0 & 0 & 0 & 1 \end{bmatrix}$$

$$= \begin{bmatrix} 0 & 2L+2L_2 & \frac{L-L_2}{\eta} & \frac{L\xi+L_2\xi-\eta^2}{\eta} \\ 0 & 2 & \frac{1}{\eta} & \frac{\xi}{\eta} \\ \frac{\xi}{\eta} & \frac{L\xi+L_1\xi-\eta^2}{\eta} & 0 & 2\xi \\ \frac{1}{\eta} & \frac{L-L_1}{\eta} & 0 & 2 \end{bmatrix} \tag{15}$$

where $\eta k = 1$ has been chosen. However, the exchange is incomplete as evidenced by the non-zero elements in the two diagonal 2×2 block matrices.

3.2 Kim EEX

An exact exchange optics was later proposed by Kim [15, 16]. Two identical dog-legs replace the chicane, as shown with dashed line scenario in Fig. 1 [19]. The transfer matrix for this beam line is $R_{d+}R_{L_2}R_kR_{L_1}R_{d+}$. Exact EEX is achieved when $\eta k = -1$. Based on this optics, experiments at FNAL [10] have been performed and others are being planned at ANL [17]. The transform map is calculated to be

$$\begin{bmatrix} 0 & 0 & -\frac{L+L_2}{\eta} & -\frac{L\xi+L_2\xi-\eta^2}{\eta} \\ 0 & 0 & -\frac{1}{\eta} & -\frac{\xi}{\eta} \\ -\frac{\xi}{\eta} & -\frac{L\xi+L_1\xi-\eta^2}{\eta} & 0 & 0 \\ -\frac{1}{\eta} & -\frac{L+L_1}{\eta} & 0 & 0 \end{bmatrix} \tag{16}$$

if $\eta k = -1$. The exchange is complete.

3.3 Xiang-Chao EEX

From a practical point of view, EEX with a chicane may be more desirable because of its minimal perturbation to existing beamlines. A chicane-type exact EEX scheme is shown in the upper figure in Fig. 2 [19]. The key to make it work is a $-I$ transformation inserted in the chicane. The transform map is found to be

$$\begin{bmatrix} 0 & 0 & \frac{L+L_2}{\eta} & \frac{L\xi+L_2\xi-\eta^2}{\eta} \\ 0 & 0 & \frac{1}{\eta} & \frac{\xi}{\eta} \\ -\frac{\xi}{\eta} & \frac{-L\xi+\eta^2}{\eta} & 0 & 0 \\ -\frac{1}{\eta} & -\frac{L}{\eta} & 0 & 0 \end{bmatrix} \tag{17}$$

when $\eta k = 1$.

Furthermore, as shown in the lower figure of Fig. 2, by inserting telescopic sections, the condition for complete exchange can be relaxed to $\eta k = 1/N$ which reduces the required strength of the transverse cavity.

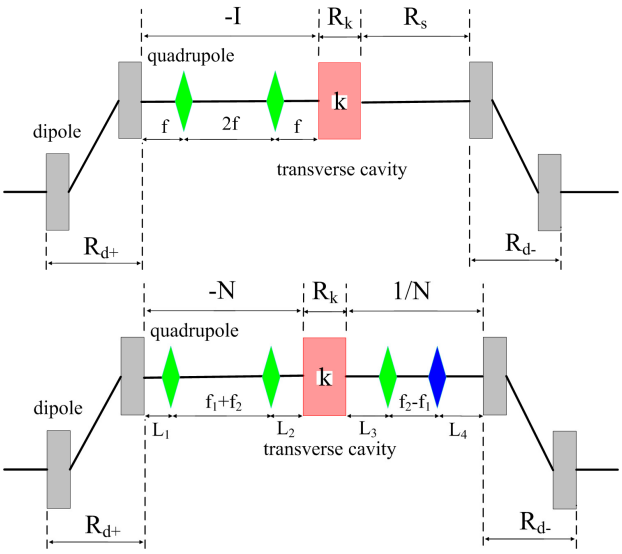

Figure 2: (Top) A chicane-type exact EEX beam line. Two quadrupoles (green diamonds) are put upstream of the transverse cavity to reverse the dispersion. (Bottom) Exact EEX beam line with $|\eta k| < 1$.

3.4 x-z Phase Space Exchanger

A clean x-z phase space exchanger can be obtained by inserting

$$\begin{bmatrix} -\frac{L}{\eta} & \frac{L\xi-\eta^2}{\eta} & 0 & 0 \\ \frac{1}{\eta} & -\frac{\xi}{\eta} & 0 & 0 \\ 0 & 0 & 1 & 0 \\ 0 & 0 & 0 & 1 \end{bmatrix}$$

upstream and inserting

$$\begin{bmatrix} \frac{\xi}{\eta} & -\frac{L\xi+L_2\xi-\eta^2}{\eta} & 0 & 0 \\ -\frac{1}{\eta} & \frac{L+L_2}{\eta} & 0 & 0 \\ 0 & 0 & 1 & 0 \\ 0 & 0 & 0 & 1 \end{bmatrix}$$

downstream the Xiang-Chao section. Then the complete map becomes

$$\begin{bmatrix} 0 & 0 & 1 & 0 \\ 0 & 0 & 0 & 1 \\ 1 & 0 & 0 & 0 \\ 0 & 1 & 0 & 0 \end{bmatrix}$$

i.e. $x \leftrightarrow z, x' \leftrightarrow \delta$, which provides a clean phase space exchanger. Note that these added insertions are straightforward, each consisting of two quadrupoles.

Note also that they are inserted external to the EEX and do not affect any of the optics within the EEX already worked out.

3.5 x-y Phase Space Exchanger

For completeness, we mention that a clean phase space exchanger between x and y was discussed before [See Eq.(14)], i.e. a solenoid with $k_s z = \pi$. The map is

$$\begin{bmatrix} 0 & 0 & 0 & \frac{2}{k_s} \\ 0 & 0 & -\frac{k_s}{2} & 0 \\ 0 & -\frac{2}{k_s} & 0 & 0 \\ \frac{k_s}{2} & 0 & 0 & 0 \end{bmatrix}$$

and it provides a clean phase space exchange $x \leftrightarrow y', x' \leftrightarrow y$.

Another simple example is to insert a quadrupole channel with

$$\begin{bmatrix} 1 & 0 & 0 & 0 \\ 0 & 1 & 0 & 0 \\ 0 & 0 & -1 & 0 \\ 0 & 0 & 0 & -1 \end{bmatrix}$$

but rotated by 45°. This insertion will produce

$$\begin{bmatrix} 0 & 0 & -1 & 0 \\ 0 & 0 & 0 & -1 \\ -1 & 0 & 0 & 0 \\ 0 & -1 & 0 & 0 \end{bmatrix}$$

3.6 Applications of x-z exchangers

As emphasized before, adapters can be envisioned for a wide range of applications. An incomplete list for x-z phase space exchangers, for example, might have the following envisioned applications [19]:

- When $\epsilon_z \ll \epsilon_x$, EEX allows small ϵ_x for FEL
- When $\epsilon_z \gg \epsilon_x$, EEX allows bunch compression
- Observing z-distribution by an x-profile monitor
- Tailoring z-distribution by an x-scraper
- Measuring slice energy spread by an x-profile monitor
- Cleaning the z- and δ-tails by an x-scraper
- Observing beam microbunching in z by an x-profile monitor
- Generating z-microbunching by modulating the x-profile of a beam
- Generating z-double bunches by an x-wire scraper

- Longitudinal phase space linearizer by a sextupole
- Study coherent synchrotron radiation (CSR) effects by converting CSR-induced z-δ correlation to x-x' correlation
- When $\epsilon_z \ll \epsilon_x$, suppress CSR in a beamline section by EEX and reversing the exchange afterwards
- Observing curvature of $z(y)$ by an x-y profile monitor in the effort to condition the beam for FEL
- Bunch compression without energy chirp

It is clear that more applications can be envisioned. A few of the above applications are detailed below.

Generating z-microbunching by modulating the x-profile of a beam Using EEX to generate sub-ps microbunch trains with a transverse multi-slit mask has been experimentally demonstrated [20]. A schematic layout is shown in Fig. 3 [19]. A mask is first used to generate density modulation in transverse direction. After the mask, a phase space exchanger is inserted to provide exact mapping $x \to z$ and $x' \to \delta$ with a unity magnification. An x-mask with 0.8 μm slits gives beam with 0.8 μm microbunches in z. Obviously, shorter microbunches can be obtained by larger x-to-z demagnification factor.

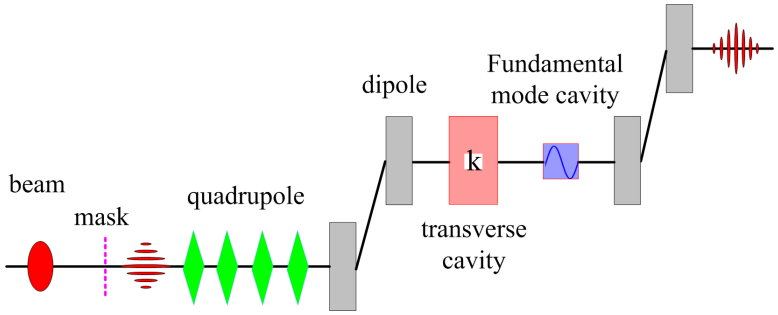

Figure 3: Schematic of a beamline to generate optical microbunch based on x-z phase space exchanger. A two-dog-leg scheme is shown in this example.

Observing curvature of $z(y)$ by an x-y profile monitor A curvature in $z(y)$ in the microbunches (as illustrated in Fig. 4(left) below) hurts the FEL mechanism and needs to be cured by beam conditioning. An x-z phase space exchanger will allow observation of $z(y)$ curvature on an x-y profile [19]. Figure 4 is a simulation of one example of this application.

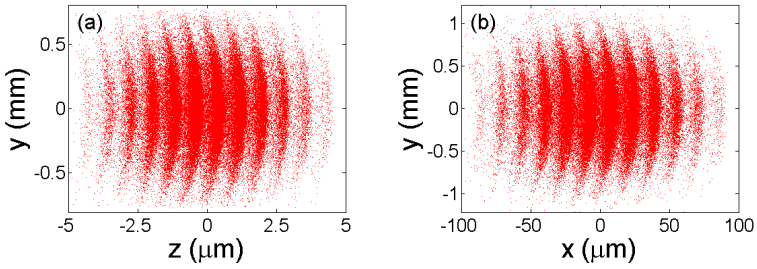

Figure 4: (Left) Initial z-y correlation; (Right) Final x-y correlation after an x-z phase space exchanging.

Bunch compression without energy chirp This idea was proposed by Zholents and Zolotorev [18]. With two back-to-back x-z phase space exchangers and a telescopic beamline in between, as illustrated in Fig. 5, a bunch compression is executed without an energy chirp as required in a conventional bunch compressor. No rf cavities are needed in this scheme, thus avoiding the associated rf nonlinearities. With back-to-back exchanges, there is no net emittance or phase space exchanges. The beam optics is described as

$$\begin{bmatrix} 0 & 0 & 1 & 0 \\ 0 & 0 & 0 & 1 \\ 1 & 0 & 0 & 0 \\ 0 & 1 & 0 & 0 \end{bmatrix} \begin{bmatrix} -N & 0 & 0 & 0 \\ 0 & -\frac{1}{N} & 0 & 0 \\ 1 & 0 & 0 & 0 \\ 0 & 1 & 0 & 0 \end{bmatrix} \begin{bmatrix} 0 & 0 & 1 & 0 \\ 0 & 0 & 0 & 1 \\ 1 & 0 & 0 & 0 \\ 0 & 1 & 0 & 0 \end{bmatrix} = \begin{bmatrix} 1 & 0 & 0 & 0 \\ 0 & 1 & 0 & 0 \\ 0 & 0 & -N & 0 \\ 0 & 0 & 0 & -\frac{1}{N} \end{bmatrix} \tag{18}$$

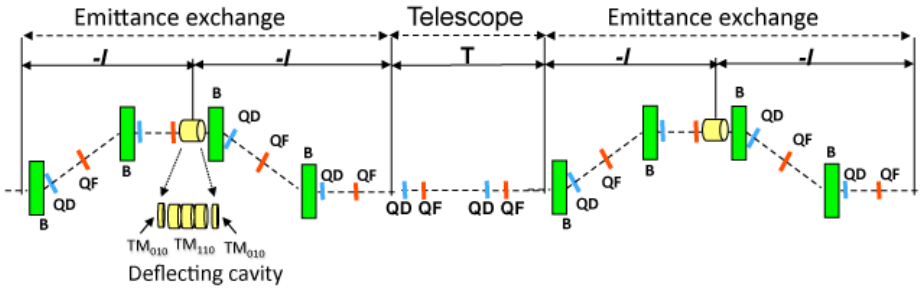

Figure 5: This scheme of two back-to-back x-z exchangers with a telescope in between provides a bunch compression without the use of transverse cavities. (Courtesy Zholents 2011)

4 Emittance partitioning

The emittance exchangers and phase space exchangers are special cases of adapters. Adapters are symplectic devices. As sympectic devices, they manipulate the phase spaces but, as a theorem in Hamiltonian beam dynamics, they do not alter the eigen-emittances [28, 29]. They can cleverly *exchange* emittances among the eigen-dimensions, but do not *change* them. In some applications, it is desirable to *change* the emittances. In such applications, emittance and phase space exchanges are not sufficient. One then seeks the help from emittance partitioning devices to be described in this section.

It should be noted that in all emittance partitioning applications, the *product* of the three eigen-emittances shall remain invariant. To illustrate the application of emittance partitioning, for example, we might consider a beam initially produced with eigen-emittances $(\epsilon_{x0}, \epsilon_{y0}, \epsilon_{z0}) = (0.4\,\mu\text{m}, 0.4\,\mu\text{m}, 4\,\mu\text{m})$ for an FEL. With an EEX device, we will be able to exchange the three values of eigen-emittances around, but will not be able to alter their values. With an emittance partitioning device, we might aim to change them to $(0.1\,\mu\text{m}, 0.1\,\mu\text{m}, 64\,\mu\text{m})$ for some FEL applications. Note that in this application, what is important is to reach $\epsilon_x = \epsilon_y = 0.1\,\mu$m. Note also that the product of the three eigen-emittances is not varied. Once available, emittance partitioners can be powerful devices.

We now have a dilemma. Since all beamline elements are necessarily symplectic, it follows from the above theorem that the beam's eigen-emittances cannot be changed once the beam was born at the cathode. It then follows that there are only two ways to design an emittance partitioner:

- Try to affect the way the beam is born at the cathode.
- If the partitioning device has to be installed after the beam is born, then it has to contain non-symplectic beamline elements.

As it stands today, there have been three proposed ways to make emittance partitioning:

- Magnetized cathode for x-y partitioning,
- Tilted laser at photocathode for x-z or y-z partitioning,
- Tapered foil for x-z or y-z partitioning.

4.1 Magnetized cathode

Consider a photocathode immersed in solenoid field B_s. Consider the case when incident laser is normal to the cathode and is cylindrically symmetric. The 4×4 beam second-moment matrix at the cathode is round, with

$$\Sigma_0 = \begin{bmatrix} \sigma_{x0}^2 & 0 & 0 & 0 \\ 0 & {\sigma'_{x0}}^2 & 0 & 0 \\ 0 & 0 & \sigma_{x0}^2 & 0 \\ 0 & 0 & 0 & {\sigma'_{x0}}^2 \end{bmatrix} \tag{19}$$

where we have used $X = (x, x', y, y')$ coordinates (instead of the canonical $X_{\rm can}$ coordinates) because that is how the beam gets produced at the cathode, even if magnetized.

As soon as the beam is born at the cathode, its eigen-emittances are determined, because, as mentioned, any subsequent symplectic beamlime element will not be able to alter their values. The eigen-emittances however are not given simply by $\sigma_{x0}\sigma'_{x0}$ as one might casually expect. To find the eigen-emittances, one must not use the X coordinates but has to use the canonical coordinates,

$$X_{\rm can} = \left(x, p_x = x' - \frac{k_s}{2} y, y, p_y = y' + \frac{k_s}{2} x \right) \tag{20}$$

where $k_s = B_s/(B\rho)$, or

$$X_{\rm can} = MX$$

where

$$M = \begin{bmatrix} 1 & 0 & 0 & 0 \\ 0 & 1 & -\frac{k_s}{2} & 0 \\ 0 & 0 & 1 & 0 \\ \frac{k_2}{2} & 0 & 0 & 1 \end{bmatrix}$$

In terms of the canonical coordinates $X_{\rm can}$, the beam matrix is

$$\Sigma_1 = M\Sigma_0 M^T \tag{21}$$

The new-born beam always has the same Σ_0 distribution in the X coordinates regardless of B_s. However, when projected to the $X_{\rm can}$ coordinates, it changes with B_s according to Σ_1. Magnetizing the cathode is therefore one way to partition the eigen-emittances. Note that the matrix M is non-symplectic.

To compute the eigen-emittances, we note that they are determined once the second-moment matrix Σ is known, and in fact are simply given by the eigen-values of $iJ\Sigma$, where J is the symplectic form

$$J = \begin{bmatrix} 0 & 1 & 0 & 0 \\ -1 & 0 & 0 & 0 \\ 0 & 0 & 0 & 1 \\ 0 & 0 & -1 & 0 \end{bmatrix}$$

Explicit calculation then gives the two eigen-emittances for Σ_1:

$$\epsilon_{1,2} = \sigma_{x0}\sqrt{{\sigma'_{x0}}^2 + \frac{k_s^2}{4}\sigma_{x0}^2} \;\pm\; \frac{k_s}{2}\sigma_{x0}^2 \tag{22}$$

Figure 6 shows the eigen-emittances (blue and purple curves) and the emittance aspect ratio ϵ_1/ϵ_2 (green curve) as functions of the parameter $\xi = k_s\sigma_{x0}/\sigma'_{x0}$. The parameter ξ controls the partitioning of the two eigen-emittances (keeping their product invariant). To produce a very flat beam (from a round laser cathode!), one takes a large value of ξ. For example, $\epsilon_1/\epsilon_2 = 1/250$ if $\xi = 8$, which might be realized for example if $\sigma_{x0}/\sigma'_{x0} = 1$ m, $B_s = 0.3$ T, $E = 100$ keV.

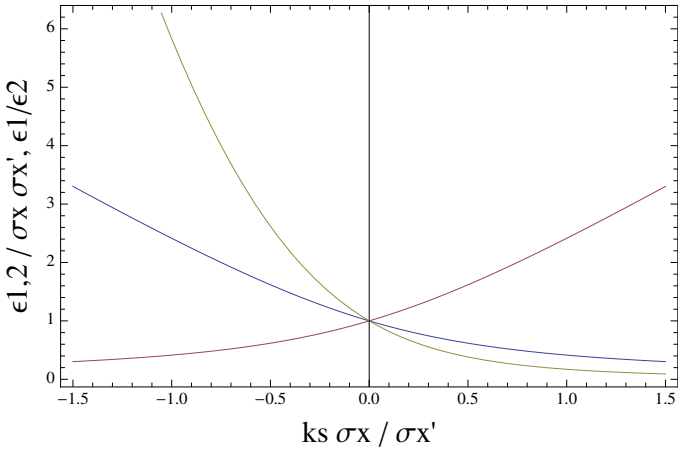

Figure 6: Emittance partitioning by immersing the electron gun in a solenoid.

By choosing appropriate values of ξ, we control the eigen-emittances after exiting the solenoid. However, at the solenoid exit, phase space is entangled. We still need to insert a round-to-flat adapter so that the eigen-planes align with x and y [30]. This adapter consists of three skew quarupoles as discussed earlier, and is symplectic, so will not further alter the eigen-emittances. The skew quadrupole channel will have to provide a map (11) with proper optical matching,

$$\frac{1}{\beta^2} \;=\; \frac{1}{\beta_y^2} \;=\; \frac{k_s^2}{4} + \frac{{\sigma'_{x0}}^2}{\sigma_{x0}^2} \tag{23}$$

Inserting this channel after the solenoid exit, the beam distribution matrix becomes diagonal,

$$\Sigma_1 = \begin{bmatrix} \sigma_{x1}^2 & 0 & 0 & 0 \\ 0 & {\sigma'_{x1}}^2 & 0 & 0 \\ 0 & 0 & \sigma_{x2}^2 & 0 \\ 0 & 0 & 0 & {\sigma'_{x2}}^2 \end{bmatrix} \tag{24}$$

and by properly choosing the solenoid strength, one of the dimensions will have a very small emittance.

4.2 Partitioning by tilted laser

Magnetized cathode is a way to partition the x- and y-emittances, leaving z-emittance intact. But how to control x- and z-emittances (leaving y-emittance intact)? One way suggested by B. Carlsten is to tilt the laser pulse-front at the photo-cathode [22, 25]. A tilted laser can be described by an equivalent coordinate mapping,

$$x \;=\; x_0$$

$$z \quad = \quad z_0 - x_0 \tan\theta \tag{25}$$

Note that the tilt is applied to the laser, not the electrons, and this coordinate correlation is non-symplectic.

The laser tilt modifies the eigen-emittances of the electron beam at its birth. Assume the beam distribution (in x-z phase space, and here we consider the coordinate system $X = (x, x', y, y')$ as we are not immersing the cathode in a solenoidal field) produced by the laser without pulse-front tilt is

$$\Sigma_0 = \begin{bmatrix} \sigma_{x0}^2 & 0 & 0 & 0 \\ 0 & {\sigma'_{x0}}^2 & 0 & 0 \\ 0 & 0 & \sigma_{z0}^2 & 0 \\ 0 & 0 & 0 & {\sigma'_{\delta 0}}^2 \end{bmatrix} \tag{26}$$

Then with the x-z correlation (25), the beam matrix becomes

$$\Sigma_1 = \begin{bmatrix} \sigma_{x0}^2 & 0 & \alpha\sigma_{x0}^2 & 0 \\ 0 & {\sigma'_{x0}}^2 & 0 & 0 \\ \alpha\sigma_{x0}^2 & 0 & \sigma_{z0}^2 + \alpha^2\sigma_{x0}^2 & 0 \\ 0 & 0 & 0 & {\sigma'_{\delta 0}}^2 \end{bmatrix} \tag{27}$$

where $\alpha = -\tan\theta$.

The eigen-emittances are readily obtained,

$$\epsilon_{1,2} = \sqrt{\frac{\sigma_{z0}^2\sigma_{\delta 0}^2 + \sigma_{x0}^2{\sigma'_{x0}}^2 + \alpha^2\sigma_{x0}^2\sigma_{\delta 0}^2 \pm \sqrt{(\sigma_{z0}^2\sigma_{\delta 0}^2 + \sigma_{x0}^2{\sigma'_{x0}}^2 + \alpha^2\sigma_{x0}^2\sigma_{\delta 0}^2)^2 - 4\sigma_{z0}^2\sigma_{\delta 0}^2\sigma_{x0}^2{\sigma'_{x0}}^2}}{2}} \tag{28}$$

The emittance aspect ratio is given by

$$\frac{\epsilon_1}{\epsilon_2} = \sqrt{\frac{t^2}{2} - 1 + t\sqrt{\frac{t^2}{4} - 1}} \tag{29}$$

with

$$t = \frac{\epsilon_{x0}}{\epsilon_{z0}} + \frac{\epsilon_{z0}}{\epsilon_{x0}} + \alpha^2\frac{\sigma_{x0}\sigma_{\delta 0}}{\sigma'_{x0}\sigma_{z0}}$$

The aspect ratio ϵ_1/ϵ_2 as a function of two parameters

$$\begin{aligned} f_0 \quad &= \quad \epsilon_{z0}/\epsilon_{x0} \\ k \quad &= \quad \alpha^2\sigma_{x0}\sigma_{\delta 0}/\sigma'_{x0}\sigma_{z0} \end{aligned}$$

is shown in Fig. 7.

Take for example normalized $\sigma_{x0} = 1.3$ mm, $\sigma'_{x0} = 0.3$ mrad, $\epsilon_{x0} = 0.4$ μm, $\sigma_{z0} = 0.8$ mm, $\sigma_{\delta 0} = 5 \times 10^{-3}$, and $\sigma_{z0} = 4$ μm, we obtain $f_0 = 10, k = 27\,\alpha^2$, and it follows that ϵ_1/ϵ_2 ranges up to 30.

As always, we still need to diagonalize the coordinates after the tilted laser gun. That is to be done by an appropriate adapter [30].

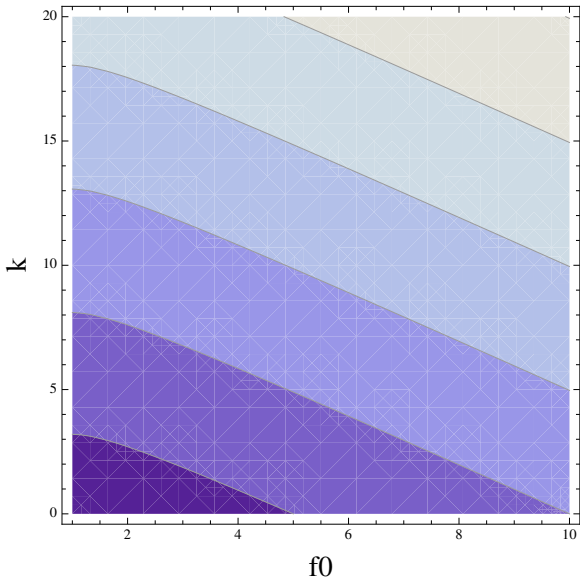

Figure 7: Contour plot of emittance aspect ratio controlled by a tilted laser front at the electron gun cathode.

4.3 Combining magnetized cathode with tilted laser

We now return to the envisioned beam emittances requirement suggested earlier, i.e.,

$$(\epsilon_{x0}, \epsilon_{y0}, \epsilon_{z0}) = (0.4\,\mu\text{m}, 0.4\,\mu\text{m}, 4\,\mu\text{m}) \quad \rightarrow \quad (0.1\,\mu\text{m}, 0.1\,\mu\text{m}, 64\,\mu\text{m})$$

Since this envisioned application involves emittance partitioning among all three dimensions, it is natural to consider now a combined configuration of a tilted laser (partitioning x and z) and a magnetized photocathode (partitioning x and y).

We need 6D analysis for this consideration. The 6D beam distribution in X_{can} coordinates is found by a straightforward calculation to be

$$\Sigma_2 = \begin{bmatrix} \sigma_{x0}^2 & 0 & 0 & \frac{k_s}{2}\sigma_{x0}^2 & \alpha\sigma_{x0}^2 & 0 \\ 0 & {\sigma'_{x0}}^2 + \frac{k_s^2}{4}\sigma_{x0}^2 & -\frac{k_s}{2}\sigma_{x0}^2 & 0 & 0 & 0 \\ 0 & -\frac{k_s}{2}\sigma_{x0}^2 & \sigma_{x0}^2 & 0 & 0 & 0 \\ \frac{k_2}{2}\sigma_{x0}^2 & 0 & 0 & {\sigma'_{x0}}^2 + \frac{k_s^2}{4}\sigma_{x0}^2 & \frac{\alpha k_s}{2}\sigma_{x0}^2 & 0 \\ \alpha\sigma_{x0}^2 & 0 & 0 & \frac{\alpha k_s}{2}\sigma_{x0}^2 & \sigma_{z0}^2 + \alpha^2\sigma_{x0}^2 & 0 \\ 0 & 0 & 0 & 0 & 0 & \sigma_{\delta 0}^2 \end{bmatrix} \tag{30}$$

Eigen-emittances are determined by

$$E^3 - (2 + f_0^2 + g^2 + h^2)E^2 + (1 + 2f_0^2 + g^2 + f_0^2 h^2)E - f_0^2 = 0 \tag{31}$$

where

$$E = \left(\frac{\epsilon}{\sigma_{x0}\sigma'_{x0}}\right)^2, g = \frac{\alpha\sigma_{\delta 0}}{\sigma'_{x0}}, f_0 = \frac{\sigma_{z0}\sigma_{\delta 0}}{\sigma_{x0}\sigma'_{x0}}, h = \frac{k_s\sigma_{x0}}{\sigma'_{x0}}$$

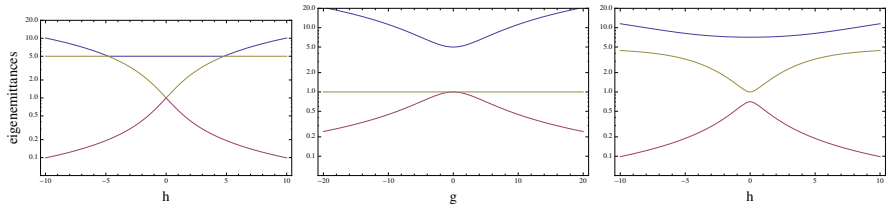

Figure 8: Illustration of emittance partitioning by combined effect of tilted laser and magnetized cathode.
(Left): Cathode magnetized but laser not tilted, with $f_0 = 5, g = 0$.
(Middle): Laser tilted but cathode not magnetized, with $f_0 = 5, h = 0$.
(Right): cathode magnetized and laser tilted $f_0 = 5, g = 5$.

Naively we might think to achieve the desired FEL emittances in two steps:

1. Tilted laser:

$$(\epsilon_{x0}, \epsilon_{y0}, \epsilon_{z0}) = (0.4\,\mu\text{m}, 0.4\,\mu\text{m}, 4\,\mu\text{m}) \quad \rightarrow \quad (0.025\,\mu\text{m}, 0.4\,\mu\text{m}, 64\,\mu\text{m})$$

2. then with immersed solenoid:

$$(0.025\,\mu\text{m}, 0.4\,\mu\text{m}, 64\,\mu\text{m}) \quad \rightarrow \quad (0.1\,\mu\text{m}, 0.1\,\mu\text{m}, 64\,\mu\text{m})$$

But as Fig. 8 shows, there is not a combination of parameters that reach the emittance design goal. This idea does not work and the reason is that both immersed solenoid and the tilted laser are applied at the cathode, not applied in sequence. Combined laser tilt and immersed solenoid can not produce the desired emittances [25].

Based on this attempt, we conclude that, with tilted laser and magnetized cathode, there are three scenarios for us to reach $\epsilon_x = \epsilon_y = 0.1\,\mu$m:

- Start with $(\epsilon_{x0}, \epsilon_{y0}, \epsilon_{z0}) = (X, Y, 0.1)$. Apply magnetized cathode to obtain $(10 * XY, 0.1, 0.1)$. Then go through x-z emittance exchanger to get $(0.1, 0.1, 10 * XY)$.
- Start with $(\epsilon_{x0}, \epsilon_{y0}, \epsilon_{z0}) = (X, 0.1, Z)$. Apply tilted laser cathode to obtain $(0.1, 0.1, 10 * XZ)$.
- Start with $((\epsilon_{x0}, \epsilon_{y0}, \epsilon_{z0}) = (0.1, Y, Z)$. Apply tilted laser cathode to obtain $(0.1, 0.1, 10 * YZ)$.

In all cases, however, at least one of the initial emittances has to be 0.1 μm. To achieve our emittance goal, we will have to give up on combining tilted laser and magnetized cathode.

4.4 Partitioning by foil

We in fact learned that combining steps at the cathode where the beam is born does not work well. Partitioning steps must be clearly separated. This means the second step, necessarily applied after the beam is born, will have to be non-symplectic. The idea, first introduced by Peterson 1983 and re-introduced by Carlsten, is to insert a tapered foil [23, 22, 30].

A tapered foil is a foil whose thickness depends on the horizontal displacement x. When inserted in the beam's passage way, a beam particle with horizontal displacement x will see a small energy loss that contains a term that is linearly dependent on x. This effect is represented by the non-symplectic map

$$\begin{bmatrix} 1 & 0 & 0 & 0 \\ 0 & 1 & 0 & 0 \\ 0 & 0 & 1 & 0 \\ S & 0 & 0 & 1 \end{bmatrix}$$

in the coordinates $X = (x, x', z, \delta)$.

Due to this tapered foil, the beam distribution

$$\Sigma_0 = \begin{bmatrix} \sigma_{x0}^2 & 0 & 0 & 0 \\ 0 & {\sigma'_{x0}}^2 & 0 & 0 \\ 0 & 0 & \sigma_{z0}^2 & 0 \\ 0 & 0 & 0 & \sigma_{\delta 0}^2 \end{bmatrix} \tag{32}$$

is transformed to

$$\Sigma_1 = \begin{bmatrix} \sigma_{x0}^2 & 0 & 0 & S\sigma_{x0}^2 \\ 0 & {\sigma'_{x0}}^2 + {\Delta\sigma'_x}^2 & 0 & 0 \\ 0 & 0 & \sigma_{z0}^2 & 0 \\ S\sigma_{x0}^2 & 0 & 0 & \sigma_{\delta 0}^2 + +S^2\sigma_{x0}^2 + {\Delta\sigma_\delta}^2 \end{bmatrix} \tag{33}$$

where ${\Delta\sigma'_x}^2$ is added to the $\langle x'^2 \rangle$ and ${\Delta\sigma_\delta}^2$ added to $\langle \delta^2 \rangle$ to model the effects of Coulomb scattering by the foil. The foil introduces three quantities: $S, {\Delta\sigma'_x}^2$and ${\Delta\sigma_\delta}^2$ — S is what the tapered foil is designed to provide, while the other two quantities are undesired but nevertheless come along with the foil unavoidably.

The x eigen-emittance is found to be

$$\epsilon_x = \sqrt{\frac{A - \sqrt{A^2 - B^2}}{2}} \tag{34}$$

where

$$\begin{aligned} A &= (\sigma'_{x0}2 + {\Delta\sigma'_x}^2)\sigma_{x0}^2 + (\sigma_{\delta 0}^2 + {\Delta\sigma_\delta}^2)\sigma_{z0}^2 + S^2\sigma_{x0}^2\sigma_{z0}^2 \\ B^2 &= 4\sigma_{x0}^2\sigma_{z0}^2({\sigma'_{x0}}^2 + {\Delta\sigma'_x}^2)(\sigma_{\delta 0}^2 + {\Delta\sigma_\delta}^2) \end{aligned}$$

Let us now assume the use of a carbon foil, and let $d_f = L_{\text{foil}}/L_{\text{rad}}$ (L_{foil} is the foil thickness at $x = 0$ and L_{rad} is the radiation length of carbon), and cut

4% of the tail particles after passage through the foil, then for $d_f < 10^{-3}$, we have [25]

$$\begin{aligned} S\sigma_{x0} &= 41.5\,\frac{d_f}{\gamma} \\ \Delta\sigma_x'^{\,2} &= 157.4\,\frac{d_f}{\gamma^2} \\ \Delta\sigma_\delta^{\,2} &= \left(35.5\,\frac{df}{\gamma}\right)^2 \end{aligned}$$

where γ is the Lorentz energy factor.

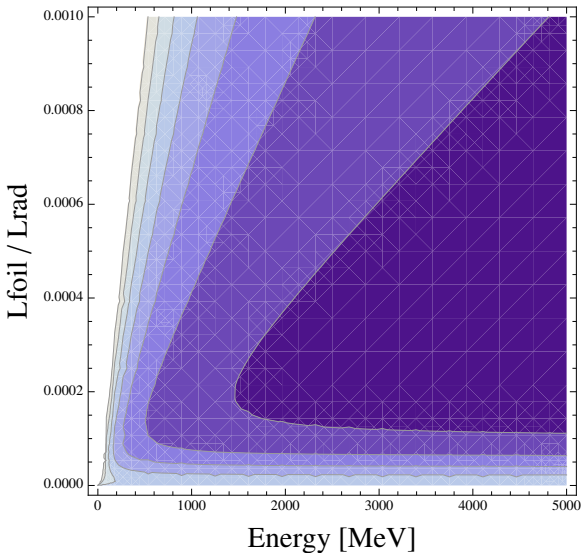

Figure 9: Contour plot of eigen-emittance with tapered foil. Input parameters are: $\sigma_{z0} = 0.5$ mm, $\sigma_{\delta 0} = 2.8$ mrad/γ, $\sigma_{x0} = 0.083$ mm/$\gamma^{1/2}$, $\sigma'_{x0} = 8.3$ mrad /$\gamma^{1/2}$. The contour lines correspond the range 0.8 – 0.5 μm for the eigen-emittance.

The result of beam emittance after the tapered foil is shown in the contour plot of Fig. 9. The beam is assumed to have initial emittances $(\epsilon_{x0}, \epsilon_{y0}, \epsilon_{z0}) = (0.7\,\mu\text{m}, 0.7\,\mu\text{m}, 1.4\,\mu\text{m})$ and we wish to reduce ϵ_x as much as possible using the tapered foil. We found that when foil scattering is included, it is difficult to lower ϵ_x to $< 0.5\,\mu$m unless much more tail particles are cut. The root cause of this difficulty is that the foil-induced energy spread $\Delta\sigma_\delta$ has become larger than the initial energy spread $\sigma_{\delta 0}$ for the needed foil thickness. In fact it was shown analytically that the best one can achieve by a tapered foil is $\epsilon_x = 63\%\,\epsilon_{x0}$ [25]. Simulations also confirmed this analytic expectation. Usefulness of tapered foil for emittance partitioning seems rather limited so far. More work is needed.

5 Summary

We have reviewed a new and powerful accelerator physics technique of phase space gymnastics. It presently contains the following topics:

- Adapters
- Emittance exchangers
- Phase space exchangers
- Emittance partitioning
  - by magnetizing the cathode
  - by tilting the photocathode laser
  - by tapered foil

This is an on-going R&D, and much studies are still being developed by the accelerator physics community.

Acknowlegments I would like to thank S. Derbenev, Y. Jiao, E. Keil, P. Raimondi, D. Ratner, D. Xiang, A. Zholents for their many helpful comments in the preparation of this review paper.

References

[1] See, for example, R. Garoby, *RF Gymnastics in a Synchrotron*, in *Handbook of Accelerator Physics and Engineering*, Ed. A.W. Chao and M. Tigner, 3rd print, p. 316, World Scientific, Singapore (2006).

[2] Y. Derbenev, Michigan Univ. Report No. 91-2 (1991); UM HE 93-20 (1993); Workshop on Round Beams and Related Concepts in Beam Dynamics, Fermilab (1996).

[3] Y. Derbenev, Michigan Univ. Report UM HE 98-04 (1998).

[4] A. Burov and V. Danilov, FNAL Report No. TM-2040 (1998); FNAL Report TM-2043 (1998).

[5] R. Brinkmann, Y. Derbenev, and K. Flöttmann, Phys. Rev. Special Topics – Accel. & Beams, 4, 053501 (2001).

[6] R. Brinkmann, Proc. European Part. Accel. Conf., TUPRI044 (2002).

[7] A. Burov, S. Nagaitsev, A. Shemyakin, and Ya. Derbenev, Phys. Rev. Special Topics – Accel. & Beams, 3, 094002 (2000).

[8] A. Burov, S. Nagaitsev, and Ysroslov Derbenev, Phys. Rev. E 66, 016503 (2002).

[9] Kwang-Je Kim, Phys. Rev. Special Topics – Accel. & Beams, 6, 104002 (2003).

[10] D. Edwards et al., Proc. 2001 Part. Accel. Conf., Chicago, IL (IEEE, Piscataway, NJ, 2001), p.73.

[11] J. Ruan, A. S. Johnson, A. H. Lumpkin, R. Thurman-Keup, H. Edwards, R. P. Fliller, T. Koeth, Y.-E Sun, Phys. Rev. Lett, 106, 244801 (2011).

[12] P. Piot, Y.-E. Sun, K.-J. Kim, Phys. Rev. Special Topics – Accel. & Beams, 9, 031001 (2006).

[13] Alexander Wu Chao and Panteleo Raimondi, SLAC-PUB-14808, unpublished (2011).

[14] M. Cornacchia and P. Emma, Phys. Rev. Special Topics – Accel. & Beams, 5, 084001 (2002).

[15] P. Emma, Z. Huang, K.-J. Kim, and P. Piot, Phys. Rev. Special Topics – Accel. & Beams, 9, 100702 (2006).

[16] K.-J. Kim, Proc. AIP Conf. No. 1086, Edt. C.B. Schröder, W. Leemans, and E. Esarey (AIP, NY, 2009).

[17] Y.-E Sun, J.G. Power, K.-J. Kim, P. Piot and M. Rihaoui, Proceedings of the 2007 Particle Accelerator Conference, Albuquerque, New Mexico (IEEE, Albuquerque, New Mexico, 2007), p.3441.

[18] A. Zholents and M. Zolotorev, *New type of a bunch compressor and generation of a short wave length coherent radiation*, SLAC Seminar (2010); Argonne National Lab. Report ANL/APS/LS-327 (2011).

[19] Dao Xiang and Alex Chao, Phys. Rev. Special Topics – Accel. & Beams, 14, 114001 (2011).

[20] Y.-E Sun, P. Piot, A. Johnson, A. H. Lumpkin, T. J. Maxwell, J. Ruan, and R. Thurman-Keup, Phys. Rev. Lett, 105, 234801 (2010).

[21] D. Xiang and Y. Ding, Phys. Rev. Special Topics – Accel. & Beams, 13, 094001 (2010).

[22] B.E. Carlsten, K.A. Bishofberger, S.J. Russell, and N.A. Yampolsky, Phys. Rev. Special Topics – Accel. & Beams, Vol. 14, 084403 (2011).

[23] J.M. Peterson, IEEE Trans. Nucl. Sci. 30, 2403 (1983).

[24] Bruce E. Carlsten et al., Phys. Rev. Special Topics – Accel. & Beams, Vol. 14, 050706 (2011).

[25] Y. Jiao, Y. Cai, and A. Chao, Proc. Intern. Part. Accel. Conf., San Sebastian, Spain, 2011.

[26] E.D. Courant and H.S. Snyder, Ann. Phys. 3, 1 (1958).

[27] See, for example, M. Bei et al., to be published in Nucl. Inst. Meth. In Phys. Res. A (2011).

[28] See, for example, E. Courant's contribution to Perspectives in Modern Physics: essays in honor of Hans A. Bethe on the occasion of his 60-th birthday, New York, Wiley, 1966.

[29] A. Dragt et al., Phys. Rev. A 45, 2572 (1992).

[30] Y. Jiao, A. Chao, Y. Cai and T. Raubenheimer, *x-z Emittance Partitioning*, SLAC seminar (2011).